Applied Physics Letters ARTICLE scitation.org/journal/apl

Application concepts for ultrafast laser-induced skyrmion creation and annihilation

Cite as: Appl. Phys. Lett. **118**, 192403 (2021); doi: 10.1063/5.0046033
Submitted: 31 January 2021 · Accepted: 26 March 2021 ·
Published Online: 11 May 2021

Kathinka Gerlinger,[1] Bastian Pfau,[1,a)] Felix Büttner,[2,3] Michael Schneider,[1] Lisa-Marie Kern,[1] Josefin Fuchs,[1] Dieter Engel,[1] Christian M. Günther,[4,5] Mantao Huang,[3] Ivan Lemesh,[3] Lucas Caretta,[3] Alexandra Churikova,[3] Piet Hessing,[1] Christopher Klose,[1] Christian Strüber,[1,b)] Clemens von Korff Schmising,[1] Siying Huang,[3] Angela Wittmann,[3] Kai Litzius,[3] Daniel Metternich,[2] Riccardo Battistelli,[2] Kai Bagschik,[6] Alexandr Sadovnikov,[7] Geoffrey S. D. Beach,[3] and Stefan Eisebitt[1,5]

AFFILIATIONS

[1]Max Born Institute for Nonlinear Optics and Short Pulse Spectroscopy, 12489 Berlin, Germany
[2]Helmholtz-Zentrum Berlin, 14109 Berlin, Germany
[3]Department of Materials Science and Engineering, Massachusetts Institute of Technology, Cambridge, Massachusetts 02139, USA
[4]Zentraleinrichtung Elektronenmikroskopie (ZELMI), Technische Universität Berlin, 10623 Berlin, Germany
[5]Institut für Optik und Atomare Physik, Technische Universität Berlin, 10623 Berlin, Germany
[6]Deutsches Elektronen-Synchrotron (DESY), 22607 Hamburg, Germany
[7]Saratov State University, Saratov 410012, Russia

Note: This paper is part of the APL Special Collection on Mesoscopic Magnetic Systems: From Fundamental Properties to Devices.
[a)]**Author to whom correspondence should be addressed:** bastian.pfau@mbi-berlin.de
[b)]Department of Physics, Freie Universität Berlin, 14195 Berlin, Germany

ABSTRACT

Magnetic skyrmions can be created and annihilated in ferromagnetic multilayers using single femtosecond infrared laser pulses above a material-dependent fluence threshold. From the perspective of applications, optical control of skyrmions offers a route to a faster and, potentially, more energy-efficient new class of information-technology devices. Here, we investigate laser-induced skyrmion generation in two different materials, mapping out the dependence of the process on the applied field and the laser fluence. We observe that sample properties like strength of the Dzyaloshinskii–Moriya interaction and pinning do not considerably influence the initial step of optical creation. In contrast, the number of skyrmions created can be directly and robustly controlled via the applied field and the laser fluence. Based on our findings, we propose concepts for applications, such as all-optical writing and deletion, an ultrafast skyrmion reshuffling device for probabilistic computing, and a combined optical and spin–orbit torque-controlled racetrack.

Since the discovery of room-temperature-stable isolated magnetic skyrmions with a chirality stabilized by interfacial Dzyaloshinskii–Moriya interaction (DMI) in ferromagnetic multilayers,[1–4] the use of these topological solitons has been discussed for data memory, storage, and processing applications.[5–8] Shifting, writing, and deleting operations were already efficiently realized exploiting spin–orbit torques (SOT) generated from spin-polarized current pulses of ns or sub-ns duration.[2,9–12] Femtosecond optical laser pulses offer an alternative way of manipulating magnetization at even shorter timescales and, potentially, with higher energy efficiency,[13] in particular when focused to a nanometer-scale spot.[14] Several groups recently reported that skyrmions form in ferromagnetic multilayers after irradiation with a single fs laser pulse.[15–17] The optical nucleation mechanism was uncovered by time-resolved x-ray scattering in concert with atomistic simulations:[16] the fs laser pulse excites the sample into a high-temperature fluctuation state that largely reduces the topological energy barrier leading to the nucleation of skyrmions on a ps timescale. This nucleation is followed by coarsening of the skyrmions to their equilibrium size and density during cooldown of the sample. Remarkably, laser nucleation of skyrmions is found in two materials that are already

considered in the research of magnetic device applications, namely Co/Pt multilayers[18] and Pt/CoFeB/MgO multilayers,[5,6,8–10] which makes laser control of nanometer-scale skyrmions attractive as an integral component in device concepts.

In the present work, we investigate optical skyrmion creation from the perspective of device applications in these two materials. Both multilayers are similar with respect to saturation magnetization and strength of the perpendicular magnetic anisotropy. As a result, both multilayers form a labyrinth of elongated domains with nanometer-scale width (stripe domains) at remanence resulting in a characteristically sheared hysteresis loop. However, the materials differ in their DMI strength: due to its sizeable DMI, Pt/CoFeB/MgO can host Neél-type skyrmions at room temperature.[2,10,19] In contrast, the domain walls in Co/Pt are predominately Bloch-type[16] as the DMI is negligible in this inversion-symmetric multilayer.

We investigate and compare laser-induced skyrmion creation in both materials by varying the applied out-of-plane magnetic field and the fluence of the infrared (IR) laser. We particularly analyze the density of skyrmion patterns created as well as correlations in the patterns. Surprisingly, we find that neither of these properties qualitatively changes with the presence or absence of DMI or pinning in the material. Most importantly, applied field and laser fluence allow for direct and robust control of the skyrmion creation, including a so far undiscovered annihilation regime. Based on this control, we propose first concepts to implement optical skyrmion creation in applications toward devices.

The experiments were conducted using Ta(3.6)/Pt(3.7)/[Pt(2.7)/$Co_{60}Fe_{20}B_{20}$(0.9)/MgO(1.5)]$_{15}$/Pt(2.7) multilayers (thicknesses in nm) and Ta(3)/[Co(0.6)/Pt(0.8)]$_{15}$/Ta(2) multilayers. Both multilayers were deposited on silicon-nitride membranes (thickness 700 nm and 150 nm, respectively) by magnetron sputtering. During deposition, the argon pressure was adjusted to 2.7×10^{-3} mbar for Co/Pt and 4×10^{-3} mbar for Pt/CoFeB/MgO (4.7×10^{-3} mbar for Pt). The Pt/CoFeB/MgO films were structured into 1.5–3 μm long and 0.9–1.4 μm wide strip lines for current injection by liftoff electron-beam lithography and focused ion beam (FIB) milling. We produced several samples with nominally identical composition. The results presented in this Letter were obtained from two Co/Pt samples and five Pt/CoFeB/MgO samples.

For Pt/CoFeB/MgO, a sizable DMI on the order of 1.8 m Jm^{-2} was previously reported[19] arising from the asymmetric interfaces of CoFeB. Due to the symmetric stacking, interface DMI contributions in Co/Pt are expected to cancel to first approximation.[3]

The magnetic hysteresis of both multilayers was measured by magneto-optical Kerr effect (MOKE) magnetometry. In the case of Co/Pt [Fig. 1(a)], we used a sister sample grown on a float glass substrate. The hysteresis of the Pt/CoFeB/MgO samples was determined on the actual striplines using a focused MOKE setup. A representative loop is shown in Fig. 1(b). The other Pt/CoFeB/MgO samples exhibit similar sheared hysteresis loops as shown in Fig. 1(b), with slightly varying saturation fields in the range of 45–65 mT due to tiny position-dependent thickness variations during the sputter deposition process.

We imaged the samples using soft x-ray Fourier-transform holography[20,21] in transmission via a standard soft x-ray holography mask, fabricated on the backside of the membrane using FIB milling, with a 1–1.5 μm field of view (FOV) and reference holes allowing for 30–40 nm spatial resolution.

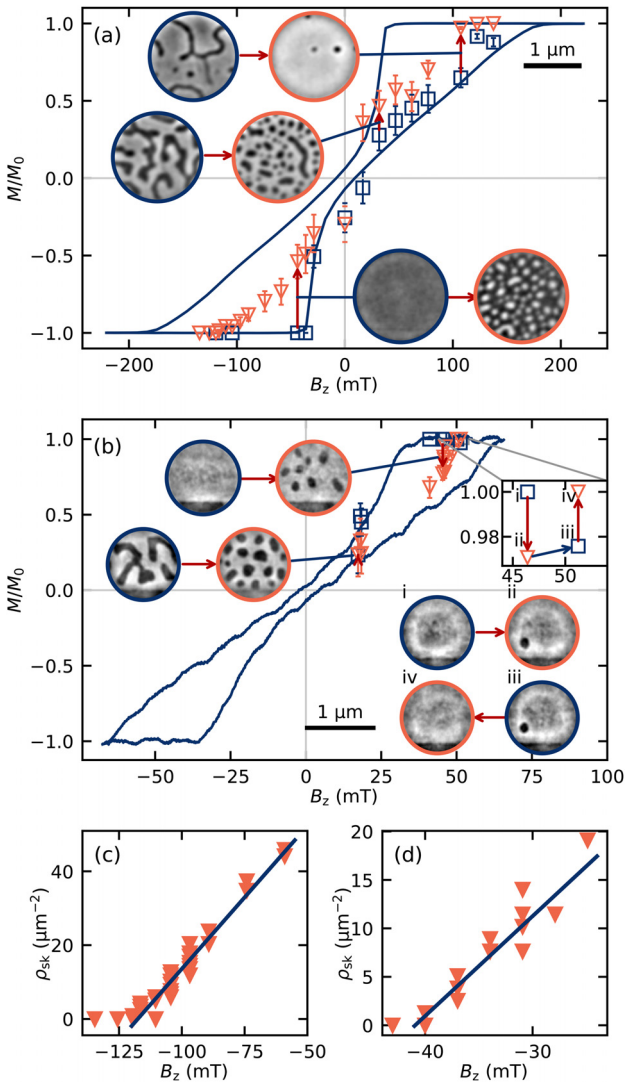

FIG. 1. Optical skyrmion creation as a function of the out-of-plane magnetic field. (a) and (b) Hysteresis curve of (a) a Co/Pt and (b) a Pt/CoFeB/MgO sample measured by MOKE (blue lines) and by holographic imaging (blue data points). Orange data points indicate the magnetization retrieved from images after irradiation with a single laser pulse. Inset images show selected examples of initial and final state pairs. The inset graph in (b) shows a single-skyrmion creation–annihilation cycle. (i) Saturated initial state, (ii) laser-induced creation of a skyrmion, (iii) same skyrmion at increased B_z, (iv) laser-induced annihilation. (c) and (d) Skyrmion density ρ_{Sk} after single-laser pulse irradiation of (c) Co/Pt and (d) Pt/CoFeB/MgO. The line represents a linear fit to the data points. (a) and (c) were measured with the same sample, (b) and (d) with different samples of the same material.

The holography experiments were conducted at beamline P04 at the synchrotron-radiation source PETRA III (Hamburg, Germany) using circularly polarized, coherent soft x-rays tuned to the cobalt L_3 edge (780 eV) to achieve magnetic contrast based on the x-ray magnetic circular dichroism. An *in situ* 1030 nm fiber laser was focused on the samples to a spot size of 60×63 μm^2 (full width at half maximum). As this size is much larger than the FOV, all fluences are given

as peak fluence of a Gaussian profile where a systematic error of up to 25% (uncertainty of the focus plane position) and a statistical error of 10% (uncertainty and drift of the sample–laser overlap) have to be considered. An out-of-plane magnetic field at the sample was applied using an electromagnet. As a typical experimental procedure, we imaged the magnetic state of the sample after (i) saturating the sample in a magnetic field of ±270 mT, (ii) reducing the field to a desired value, and (iii) applying a single 250 fs long IR laser pulse to nucleate skyrmions in the sample.

From the images of the samples' out-of-plane magnetization component (for examples, see Figs. 1 and 2), we determined the number and individual positions of the skyrmions created as well as the net magnetization within our FOV. To this end, we created binary images of up and down magnetization from the holography images using image segmentation based on Otsu's method.[22] The effective diameter d of a skyrmion was determined from its occupied area A as $d = 2\sqrt{A/\pi}$. We estimate the error to be ±2 pixels (∼20 nm), which accounts for our imaging resolution and errors from the image segmentation.

We find that skyrmions can be created in both materials after irradiation with a single suitably intense laser pulse, see Figs. 1(a) and 1(b) and Ref. 16, where the same or sister samples have been investigated, for the proof that they are skyrmions. To study the process at different initial states in the hysteresis, we recorded sets of images before and after irradiation with a single laser pulse of 19 mJ cm^{-2} at different applied fields. We distinguish four regimes of the process [inset images in Figs. 1(a) and 1(b) show prominent examples]. In the first regime, we create disordered configurations of skyrmions from an initially saturated state. Here, the final states always contain only skyrmions. We observe that the final skyrmion density in both samples is directly controlled via the applied field, allowing to cover the range from dense arrays down to single skyrmions in the FOV [Figs. 1(c) and 1(d)]. Importantly, in this regime, we find a linear relationship between skyrmion density and applied field for both materials. In the second regime, when starting from a stripe-domain state, mixed states of skyrmions coexisting with stripe domains appear after laser exposure in Co/Pt. In contrast, pure skyrmion states are still created in Pt/CoFeB/MgO, probably stabilized by the sizeable DMI in this multilayer. At remanence (third regime), without a symmetry-breaking field, the system remains in a pure stripe-domain state even after powerful laser irradiation (see Ref. 16). Close to saturation (fourth regime), we find the opposite process to skyrmion creation: a single laser pulse annihilates skyrmions and stripe domains. The graph inset of Fig. 1(b) illustrates a scheme to realize all-optical skyrmion creation and annihilation in a single device (corresponding images are shown as insets i–iv). First, starting in a saturated state at 45 mT, we optically create a single skyrmion (i→ii), then we slightly increase the field to 51 mT which still preserves the existing skyrmion (ii→iii), and finally we optically annihilate the skyrmion by a second laser pulse (iii→iv).

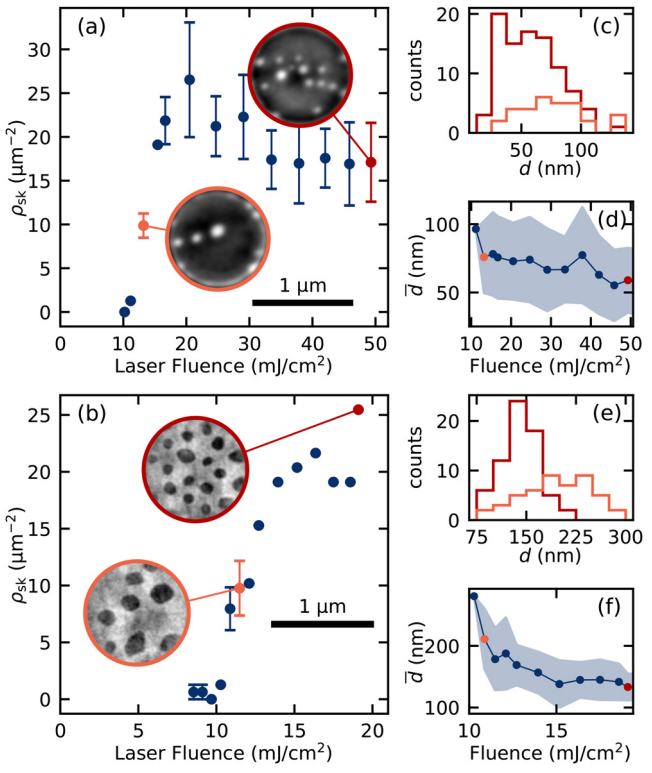

FIG. 2. Optical skyrmion creation as a function of the laser fluence. (a) and (b) Average skyrmion density after illuminating a magnetically saturated state with a single laser pulse in (a) Co/Pt (at −59 mT) and (b) Pt/CoFeB/MgO (at 20 mT). The data are based on (a) 68 images and (b) 20 images. For multiple measurements, error bars indicate their standard deviation. Inset images show two examples at low and high fluence. (c) and (e) Distribution of skyrmion diameter at low and high fluence as marked by color. (d) and (f) Average skyrmion diameter $\bar{d}$ (data points) and width of the distribution (σ_d) (filled area).

Investigating the fluence dependence of the optical skyrmion creation, we reproduce previous observations of a sharp fluence threshold in both samples [Figs. 2(a) and 2(b)]. Below the sample-specific threshold, skyrmions do not nucleate or only after thousands of laser pulses.[16] At the threshold, the skyrmion density rapidly increases with the fluence and saturates at higher fluences. The reason for this behavior is that skyrmions are nucleated in a high-temperature fluctuation phase, a process that is independent of the fluence above a threshold value.[16] After a subsequent coarsening phase during cooldown, the skyrmions' equilibrium density is determined by the applied field. The threshold for both samples is very similar with ∼13 mJ cm^{-2} for Co/Pt and ∼11 mJ cm^{-2} for Pt/CoFeB/MgO.

For applications, a narrow distribution of skyrmion diameters is desirable, in particular, if the readout relies on the anomalous Hall effect.[23] In Figs. 2(c) and 2(e), we show the diameter distribution for the threshold and saturation regime corresponding to the insets in Figs. 2(a) and 2(b). The mean ($\bar{d}$) and standard deviation (σ_d) of the distribution are plotted for all fluences in Figs. 2(d) and 2(f). The skyrmions are generally smaller in Co/Pt ($\bar{d}$ = 55–80 nm) than in Pt/CoFeB/MgO ($\bar{d}$ = 130–215 nm) which is a result of the sample-specific interplay of all magnetization-related energies.[11] In both samples, the diameter distribution of the laser-induced skyrmions is almost independent of the laser fluence. Only at very low fluences, closer to the fluence threshold, the skyrmions grow larger. As main difference between both materials, the normalized diameter variation $\sigma_d/\bar{d}$ is broader in Co/Pt (0.41) than in Pt/CoFeB/MgO (0.23).

This difference may be related to the different pinning in both samples. Co/Pt multilayers typically exhibit a high density of pinning sites due to grain boundaries and different grain orientation in the polycrystalline material.[24,25] On the contrary, CoFeB layers grow in an

amorphous way with low pinning density.[2,9,26,27] In the coarsening phase of the optical skyrmion creation process,[16] the higher pinning in Co/Pt could lead to an inhomogeneous growth of the skyrmions.

An important aspect for the application of skyrmion creation mechanisms is if and how the positions of the skyrmions created are defined in the multilayer film. For instance, natural and artificial pinning sites were used to localize SOT-induced skyrmion nucleation.[10] We therefore investigate if pinning or pre-existing magnetic textures influence the position of optically created skyrmions by evaluating the statistical spatial distribution of nucleation sites. To this end, we calculate the pair correlation between two binary images by $C = \langle m_1, m_2 \rangle / (||m_1|| \, ||m_2||)$ where $\langle ., . \rangle$ denotes the pixel-wise scalar product and $||.||$ is the corresponding norm. For m_1 and m_2, we use the normalized (binary) magnetization in each pixel reduced by the average magnetization in the FOV to account for a systematic correlation offset arising for a non-zero net magnetization from the binarization of the magnetization to the values −1 or 1. Finally, we determine the average of the correlations of all subsequent image pairs.

By applying this correlation analysis to independently created skyrmion patterns (from the data used for Fig. 2), we search for preferred nucleation sites due to pinning (red data points in Fig. 3). For Co/Pt, sufficient data are available for a fluence-resolved analysis; for Pt/CoFeB/MgO, we summarize all data above the threshold to a single correlation value. Additional sum images of the binary images illustrate the spatial distribution of nucleation sites. For both materials, we find negligible correlation ($C < 0.1$) reflecting an almost completely random and homogeneous distribution of nucleation sites from which we conclude that pinning does not play a role for the specific positions of the skyrmions created. This finding is in line with the recently proposed nucleation mechanism via a high-temperature fluctuation state that dispenses with particular nucleation sites and promotes a random distribution.[16]

To investigate the influence of pre-existing magnetic textures, we changed our experimental procedure. We started in a laser-generated skyrmion state and reimaged it after each subsequent laser pulse without saturating the sample in between. We recorded five images after subsequent laser pulses per fluence and show the average correlation in Fig. 3 as blue data points. Here, we find a different behavior than before: at fluences above, but close to the nucleation threshold, the correlation is very high, meaning that the initially created skyrmion pattern is to a large extent reproduced after a subsequent laser pulse of the same intensity. In contrast, at high fluences significantly exceeding the nucleation threshold, the skyrmion positions become completely uncorrelated and distribute almost homogeneously over the FOV. This second, softer fluence threshold was missed in the previous studies of laser-induced skyrmion nucleation. We explain the memory effect at lower fluence with an inhomogeneous excitation along the depth of the sample due to the strong absorption of the IR in the multilayers. At low fluences, it seems likely that only the topmost layers enter the fluctuation state while patterns in the lower layers, if present, are not completely erased and subsequently serve as a guide for the nucleation of the skyrmion state.

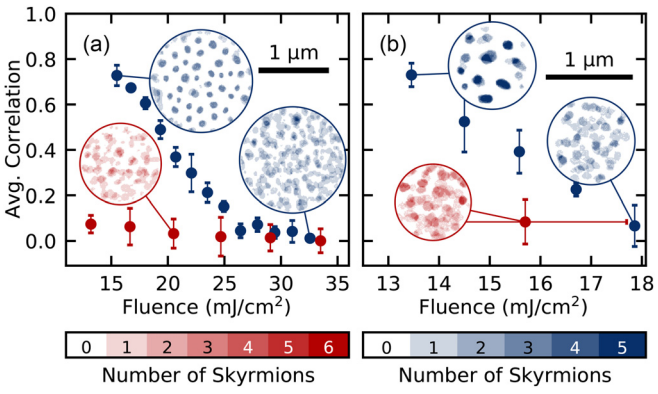

FIG. 3. Shot-to-shot correlation of created skyrmion patterns. Average correlation of skyrmion patterns in (a) Co/Pt and (b) Pt/CoFeB/MgO. Red data points show the average correlation of the data in Figs. 2(a) and 2(d) where the sample was saturated after each pulse. Blue data points show the average of at least five binary magnetization images after subsequent laser pulses without saturating the sample in between [(a) at −83 mT and (b) at 20 mT]. Insets show corresponding sum images.

The full randomization of the skyrmion pattern at high laser fluences promises a route to an interesting application of optical skyrmion writing: a skyrmion reshuffler[28,29] working on ultrafast timescales in contrast to previous proposals based on skyrmion diffusion.[5] A reshuffling device is a key component in probabilistic computing for signal decorrelation. Correlated inputs to logic gates of probabilistic computing lead to incorrect results. As the skyrmion density in the optical device is well controlled by the applied field only and is independent of the laser fluence, a single laser shot sufficiently above the skyrmion creation threshold may be used for reshuffling on the sub-ns timescale.

Summarizing our observations, we find very similar properties of both materials with respect to optical skyrmion creation, in spite of the different strength of DMI and pinning in our samples. In both materials, skyrmions are created after a single laser pulse of sufficient fluence with a density that can be controlled via the applied field, down to the generation of isolated skyrmions. At high fields, skyrmions can be annihilated in both materials. Above the fluence threshold, skyrmion diameter and density do not depend on the fluence anymore. The nucleation is spatially homogeneous without any preferred nucleation sites.

Although skyrmions can be created in both types of multilayers, the inversion-asymmetry of the Pt/CoFeB/MgO system offers additional perspectives toward opto-spintronics applications. As illustrated in Fig. 4, this material allows combining optical and SOT control of skyrmions in a single device operated at a constant bias field. To demonstrate this, we start with a saturated sample at $B_z = 42$ mT. At this field, optical skyrmion creation is impossible in this specific sample. However, a single, 4 ns long current pulse with a current density of 7×10^{11} A m^{-2} sent through the strip line still creates a single skyrmion in the FOV via SOT.[10] In the next step, we reduced the current density below the SOT nucleation threshold and applied pulse trains of positive and negative polarity to shift the skyrmion back and forth. The skyrmion moves along the current direction with the typical inclination resulting from the skyrmion Hall effect.[9,30] At the end of the series, we annihilated the skyrmion with a single laser pulse. Note that all the steps of skyrmion creation, displacement, and annihilation were performed at constant external magnetic field facilitating application in a device.

In conclusion, we demonstrate creation and annihilation of skyrmions for both kinds of ferromagnetic multilayers used in this study.

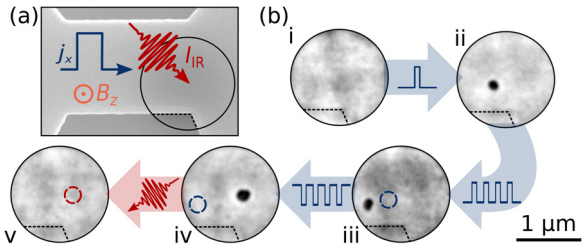

FIG. 4. Combined optical and SOT manipulation of a skyrmion in a magnetic strip line. (a) Scanning electron micrograph of the Pt/CoFeB/MgO strip line. The circle marks the FOV of holography imaging. Current pulses with density j_x are injected along the strip line. A constant bias field B_z is applied in the out-of-plane direction. The IR laser with fluence I_{IR} impinges on the material under normal incidence. (b) Sequence of images for skyrmion manipulation with SOT and fs laser pulses: (i) after saturation the field is decreased to $B_z = 42$ mT, (ii) a skyrmion is created by current pulse of $j_x = 7 \times 10^{11}$ A m^{-2}, (iii) and (iv) back and forth shifting of the skyrmion by current pulses of $j_x = 5 \times 10^{11}$–6×10^{11} A m^{-2} of different polarity, (v) annihilation of the skyrmion via a laser pulse of $I_{IR} = 32$ mJ cm^{-2}. In (iii)–(v), the previous position of the skyrmion is marked by a colored circle.

The tunability of the skyrmion density by the external magnetic field provides a critical parameter for skyrmion based applications. The skyrmion density is largely insensitive to the laser fluence above a material-dependent threshold. When laser-exposing an existing skyrmion pattern, we find a strong memory effect of the skyrmion positions at low fluences which almost completely vanishes at high fluences leading to a random distribution. We propose three application concepts based on these findings: an all-optical skyrmion writer and deleter (Fig. 1), an ultrafast skyrmion reshuffler for probabilistic computing (Fig. 3), and an opto-spintronic skyrmion racetrack (Fig. 4).

We acknowledge DESY (Hamburg, Germany), a member of the Helmholtz Association HGF, for the provision of experimental facilities. Parts of this research were carried out at PETRA III beamline P04. We thank M. Wieland and M. Drescher, Universität Hamburg, for providing us with their mobile laser hutch for the experiments at PETRA III. Work at MIT was supported by the DARPA TEE program. Devices were fabricated using equipment in the MIT Microsystems Technology Laboratory and the MIT Nanostructures Laboratory. Financial support from the Leibniz Association via Grant No. K162/2018 (OptiSPIN), the Helmholtz Young Investigator Group Program, as well as from the NSF Graduate Research Fellowship Program, the GEM Consortium, Swiss National Science Foundation and the Russian Ministry of Education and Science (Project No. FSRR-2020-0005) is acknowledged.

DATA AVAILABILITY

The data that support the findings of this study are available from the corresponding author upon reasonable request.

REFERENCES

[1]W. Jiang, P. Upadhyaya, W. Zhang, G. Yu, M. B. Jungfleisch, F. Y. Fradin, J. E. Pearson, Y. Tserkovnyak, K. L. Wang, O. Heinonen, S. G. Te Velthuis, and A. Hoffmann, "Blowing magnetic skyrmion bubbles," Science **349**, 283–286 (2015).

[2]S. Woo, K. Litzius, B. Krüger, M. Y. Im, L. Caretta, K. Richter, M. Mann, A. Krone, R. M. Reeve, M. Weigand, P. Agrawal, I. Lemesh, M. A. Mawass, P. Fischer, M. Kläui, and G. S. Beach, "Observation of room-temperature magnetic skyrmions and their current-driven dynamics in ultrathin metallic ferromagnets," Nat. Mater. **15**, 501–506 (2016).

[3]C. Moreau-Luchaire, C. Moutafis, N. Reyren, J. Sampaio, C. A. F. Vaz, N. Van Horne, K. Bouzehouane, K. Garcia, C. Deranlot, P. Warnicke, P. Wohlhüter, J.-M. George, M. Weigand, J. Raabe, V. Cros, and A. Fert, "Additive interfacial chiral interaction in multilayers for stabilization of small individual skyrmions at room temperature," Nat. Nanotechnol. **11**, 444–448 (2016).

[4]O. Boulle, J. Vogel, H. Yang, S. Pizzini, D. de Souza Chaves, A. Locatelli, T. O. Menteş, A. Sala, L. D. Buda-Prejbeanu, O. Klein, M. Belmeguenai, Y. Roussigné, A. Stashkevich, S. M. Chérif, L. Aballe, M. Foerster, M. Chshiev, S. Auffret, I. M. Miron, and G. Gaudin, "Room-temperature chiral magnetic skyrmions in ultrathin magnetic nanostructures," Nat. Nanotechnol. **11**, 449–454 (2016).

[5]J. Zázvorka, F. Jakobs, D. Heinze, N. Keil, S. Kromin, S. Jaiswal, K. Litzius, G. Jakob, P. Virnau, D. Pinna, K. Everschor-Sitte, L. Rózsa, A. Donges, U. Nowak, and M. Kläui, "Thermal skyrmion diffusion used in a reshuffler device," Nat. Nanotechnol. **14**, 658–661 (2019).

[6]S. Zhang, A. A. Baker, S. Komineas, and T. Hesjedal, "Topological computation based on direct magnetic logic communication," Sci. Rep. **5**, 15773 (2015).

[7]A. Fert, V. Cros, and J. Sampaio, "Skyrmions on the track," Nat. Nanotechnol. **8**, 152–156 (2013).

[8]R. Wiesendanger, "Nanoscale magnetic skyrmions in metallic films and multilayers: A new twist for spintronics," Nat. Rev. Mater. **1**, 16044 (2016).

[9]K. Litzius, I. Lemesh, B. Krüger, P. Bassirian, L. Caretta, K. Richter, F. Büttner, K. Sato, O. A. Tretiakov, J. Förster, R. M. Reeve, M. Weigand, I. Bykova, H. Stoll, G. Schütz, G. S. Beach, and M. Klaüi, "Skyrmion Hall effect revealed by direct time-resolved X-ray microscopy," Nat. Phys. **13**, 170–175 (2017).

[10]F. Büttner, I. Lemesh, M. Schneider, B. Pfau, C. M. Günther, P. Hessing, J. Geilhufe, L. Caretta, D. Engel, B. Krüger, J. Viefhaus, S. Eisebitt, and G. S. Beach, "Field-free deterministic ultrafast creation of magnetic skyrmions by spin-orbit torques," Nat. Nanotechnol. **12**, 1040–1044 (2017).

[11]F. Büttner, I. Lemesh, and G. S. Beach, "Theory of isolated magnetic skyrmions: From fundamentals to room temperature applications," Sci. Rep. **8**, 4464 (2018).

[12]S. Woo, K. M. Song, X. Zhang, M. Ezawa, Y. Zhou, X. Liu, M. Weigand, S. Finizio, J. Raabe, M.-C. Park, K.-Y. Lee, J. W. Choi, B.-C. Min, H. C. Koo, and J. Chang, "Deterministic creation and deletion of a single magnetic skyrmion observed by direct time-resolved X-ray microscopy," Nat. Electron. **1**, 288–296 (2018).

[13]C. D. Stanciu, F. Hansteen, A. V. Kimel, A. Kirilyuk, A. Tsukamoto, A. Itoh, and T. Rasing, "All-optical magnetic recording with circularly polarized light," Phys. Rev. Lett. **99**, 047601 (2007).

[14]M. Finazzi, M. Savoini, A. R. Khorsand, A. Tsukamoto, A. Itoh, L. Duò, A. Kirilyuk, T. Rasing, and M. Ezawa, "Laser-induced magnetic nanostructures with tunable topological properties," Phys. Rev. Lett. **110**, 177205 (2013).

[15]S. G. Je, P. Vallobra, T. Srivastava, J. C. Rojas-Sánchez, T. H. Pham, M. Hehn, G. Malinowski, C. Baraduc, S. Auffret, G. Gaudin, S. Mangin, H. Béa, and O. Boulle, "Creation of magnetic skyrmion bubble lattices by ultrafast laser in ultrathin films," Nano Lett. **18**, 7362–7371 (2018).

[16]F. Büttner, B. Pfau, M. Böttcher, M. Schneider, G. Mercurio, C. M. Günther, P. Hessing, C. Klose, A. Wittmann, K. Gerlinger, L.-M. Kern, C. Strüber, C. von Korff Schmising, J. Fuchs, D. Engel, A. Churikova, S. Huang, D. Suzuki, I. Lemesh, M. Huang, L. Caretta, D. Weder, J. H. Gaida, M. Möller, T. R. Harvey, S. Zayko, K. Bagschik, R. Carley, L. Mercadier, J. Schlappa, A. Yaroslavtsev, L. Le Guyarder, N. Gerasimova, A. Scherz, C. Deiter, R. Gort, D. Hickin, J. Zhu, M. Turcato, D. Lomidze, F. Erdinger, A. Castoldi, S. Maffessanti, M. Porro, A. Samartsev, J. Sinova, C. Ropers, J. H. Mentink, B. Dupé, G. S. D. Beach, and S. Eisebitt, "Observation of fluctuation-mediated picosecond nucleation of a topological phase," Nat. Mater. **20**, 30–37 (2021).

[17]N. Novakovic-Marinkovic, M.-A. Mawass, O. Volkov, P. Makushko, W. D. Engel, D. Makarov, and F. Kronast, "From stripes to bubbles: Deterministic transformation of magnetic domain patterns in Co/Pt multilayers induced by laser helicity," Phys. Rev. B **102**, 174412 (2020).

[18]T. R. Albrecht, H. Arora, V. Ayanoor-Vitikkate, J. Beaujour, D. Bedau, D. Berman, A. L. Bogdanov, Y. Chapuis, J. Cushen, E. E. Dobisz, G. Doerk, H. Gao, M. Grobis, B. Gurney, W. Hanson, O. Hellwig, T. Hirano, P. Jubert, D. Kercher, J. Lille, Z. Liu, C. M. Mate, Y. Obukhov, K. C. Patel, K. Rubin, R. Ruiz, M. Schabes, L. Wan, D. Weller, T. Wu, and E. Yang, "Bit-patterned magnetic recording: Theory, media fabrication, and recording performance," IEEE Trans. Magn. **51**, 1–42 (2015).
[19]I. Lemesh, K. Litzius, M. Böttcher, P. Bassirian, N. Kerber, D. Heinze, J. Zázvorka, F. Büttner, L. Caretta, M. Mann, M. Weigand, S. Finizio, J. Raabe, M.-Y. Im, H. Stoll, G. Schütz, B. Dupé, M. Kläui, and G. S. D. Beach, "Current-induced skyrmion generation through morphological thermal transitions in chiral ferromagnetic heterostructures," Adv. Mater. **30**, 1805461 (2018).
[20]S. Eisebitt, J. Lüning, W. F. Schlotter, M. Lörgen, O. Hellwig, W. Eberhardt, and J. Stöhr, "Lensless imaging of magnetic nanostructures by X-ray spectroholography," Nature **432**, 885–888 (2004).
[21]B. Pfau and S. Eisebitt, "X-ray holography," *Synchrotron Light Sources and Free-Electron Lasers* (Springer Cham, 2015).
[22]N. Otsu, "A threshold selection method from gray-level histograms," IEEE Trans. Syst., Man, Cybern. **9**, 62–66 (1979).
[23]D. Maccariello, W. Legrand, N. Reyren, K. Garcia, K. Bouzehouane, S. Collin, V. Cros, and A. Fert, "Electrical detection of single magnetic skyrmions in metallic multilayers at room temperature," Nat. Nanotechnol. **13**, 233–237 (2018).
[24]B. Pfau, C. M. Günther, E. Guehrs, T. Hauet, H. Yang, L. Vinh, X. Xu, D. Yaney, R. Rick, S. Eisebitt, and O. Hellwig, "Origin of magnetic switching field distribution in bit patterned media based on pre-patterned substrates," Appl. Phys. Lett. **99**, 062502 (2011).
[25]T. Thomson, G. Hu, and B. D. Terris, "Intrinsic distribution of magnetic anisotropy in thin films probed by patterned nanostructures," Phys. Rev. Lett. **96**, 257204 (2006).
[26]C. Burrowes, N. Vernier, J.-P. Adam, L. Herrera Diez, K. Garcia, I. Barisic, G. Agnus, S. Eimer, J.-V. Kim, T. Devolder, A. Lamperti, R. Mantovan, B. Ockert, E. E. Fullerton, and D. Ravelosona, "Low depinning fields in Ta-CoFeB-MgO ultrathin films with perpendicular magnetic anisotropy," Appl. Phys. Lett. **103**, 182401 (2013).
[27]F. Büttner, C. Moutafis, A. Bisig, P. Wohlhüter, C. M. Günther, J. Mohanty, J. Geilhufe, M. Schneider, C. v Korff Schmising, S. Schaffert, B. Pfau, M. Hantschmann, M. Riemeier, M. Emmel, S. Finizio, G. Jakob, M. Weigand, J. Rhensius, J. H. Franken, R. Lavrijsen, H. J. M. Swagten, H. Stoll, S. Eisebitt, and M. Kläui, "Magnetic states in low-pinning high-anisotropy material nanostructures suitable for dynamic imaging," Phys. Rev. B **87**, 134422 (2013).
[28]D. Pinna, F. Abreu Araujo, J.-V. Kim, V. Cros, D. Querlioz, P. Bessiere, J. Droulez, and J. Grollier, "Skyrmion gas manipulation for probabilistic computing," Phys. Rev. Appl. **9**, 064018 (2018).
[29]T. Nozaki, Y. Jibiki, M. Goto, E. Tamura, T. Nozaki, H. Kubota, A. Fukushima, S. Yuasa, and Y. Suzuki, "Brownian motion of skyrmion bubbles and its control by voltage applications," Appl. Phys. Lett. **114**, 012402 (2019).
[30]W. Jiang, X. Zhang, G. Yu, W. Zhang, X. Wang, M. Benjamin Jungfleisch, J. E. Pearson, X. Cheng, O. Heinonen, K. L. Wang, Y. Zhou, A. Hoffmann, and S. G. Te Velthuis, "Direct observation of the skyrmion Hall effect," Nat. Phys. **13**, 162–169 (2017).